31st Congress of the International Council of the Aeronautical Sciences
Belo Horizonte, Brazil; September 09-14, 2018

CALCULATION OF WATER FILM FLOW AND HEAT TRANSFER ON THE AIRCRAFT ANTI-ICING SURFACE

Mei Zheng, Tao Wu, Zhiqiang Guo, Wei Dong
Shanghai Jiao Tong University

Keywords: *water film, breakup, heat transfer, anti-icing surface, computational method*

Abstract

The runback water flow and heat transfer on the surface of aircraft components has an important influence on the design of anti-icing system. The aim of this paper is to investigate the flow and heat transfer on the anti-icing system and its influence factors, especially the film flow and the formation of rivulet. A mathematical model is developed to predict the thickness of water film and the shape of rivulet flow when the transition appears from film to rivulets. Both of the runback water layer and the external air flow boundary are subject to mass, momentum and energy conservations in the model. The effect of the contact angle is studied. The results indicate that both of the rivulet thickness and width reduce with the contact angle increasing and the rivulet width is more sensitive to the contact angle than the width.

1 Introduction

Ice accretion on aircraft may significantly change the aerodynamic characteristics and thus has a considerable effect on aircraft performance [1]. The anti-icing systems are usually used to protect aircraft from icing by heating the component surface and evaporating the impinging supercooled water droplets. When the heating energy cannot evaporate all of the impinging droplets, a water film will form on the anti-icing surface and runback due to aerodynamic forces. In order to predict the required anti-icing heating energy in the design of anti-icing systems better, an accurate model of water flow on the anti-icing surface for the anti-icing performance analysis is necessary.

Many efforts have been conducted in the numerical simulation to predict the flow and heat transfer of runback water on anti-icing surface. The heat transfer and mass balance equations on anti-icing surface would be solved simultaneously when the liquid film is coupled with ice layer growth, airflow boundary layer or the component surfaces [2-6]. Silva et al. [7] presented a mathematical model of runback water flow using the first law of thermodynamics and the mass and momentum conservation principles, which took variable properties, pressure and temperature gradients on the surface, coupled heat and mass transfer effects, and laminar to turbulent transition region modeling into consideration. Nicholas [8] presented a novel de-icing/anti-icing fluid flow-off prediction model that only considered the influence of the aerodynamic shear forces but no wave formation, which is caused by the air pressure gradients when the film thickness exceeds a certain critical value [9]. Due to the surface tension, the film flow on the anti-icing surfaces is unstable and divided into several rivulets. Al-Khalil et al. [10] developed a computing simulation for “running wet” and evaporation aircraft anti-icing system to describe the flow characteristics of water film/rivulets on aircraft surfaces. This mathematical model contained the energy balance on the metal skin, as well as the mass and energy balance on the runback water. The criteria had been applied to judge the film breakup and rivulet formation, including mass conservation, energy conservation and the minimum total energy (MTE). The MTE was used to determine the minimum wetting rate and the minimum thickness of a flowing down liquid film driven by gravity on a vertical surface [11, 12] and it also

had been applied to investigating the breakup of a thin liquid film flowing on a vertical or inclined surface which was subject to interfacial shear stress [13]. The results showed that the dimensionless liquid film thickness and wetting rate were both related to the equilibrium contact angle. Silva et al. [14, 15] considered the effects of convection and evaporation on the water film breakup and rivulets formation and then simulated the heat transfer mechanisms by the rivulets mathematical model on thermal anti-icing surfaces.

The physical behaviors of water film and related heat and mass transfer under icing conditions are very complex. Modeling the runback water film/rivulet flow is the purpose of this paper. A mathematical model for the mass and heat transfer of the water film flow on anti-icing surface is developed. The thickness distribution of the water film flow is derived. The mathematical model also considers the breakup of film and the formation of rivulets. The characteristics of the runback water under different contact angles are described and analyzed.

2 Mathematical Model

When the water droplets impinge on the anti-icing surface, a thin water film will form and run back along the surface. The continuous liquid film commonly exists in impingement regions, where the water droplets impact on intensively. When moving downstream, the film may break up and develop into individual rivulets with the influences of the pressure gradient, shear force, evaporation, and surface tension, as shown in Fig. 1.

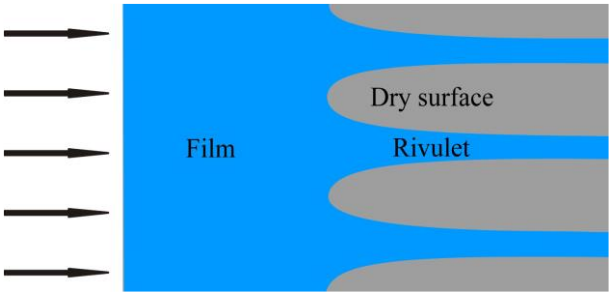

Fig. 1. Water Film Flow and Rivulets Flow

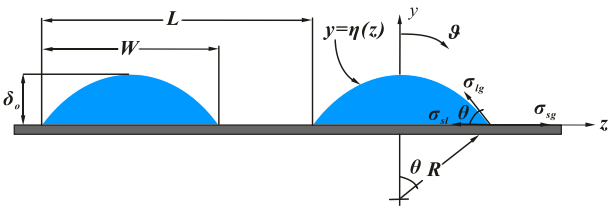

Fig. 2. Rivulet Model

The cross-section shape of a fully developed rivulet is illustrated in Fig. 2. The rivulet moving is driven by the viscous shear force acting on rivulet free surface. The shape of the rivulet is dominated by surface tension and the liquid-gas interface can be determined as:

$$y = \eta(z) = R(\cos\vartheta - \cos\theta) \quad \vartheta \in [0, \theta] \tag{1}$$

where R represents the radius of the rivulet cross-section which is assumed as a segment of a cylinder. θ is the contact angle and the contact line is subject to the tensions of three surfaces, namely the solid-gas, the solid-liquid and the liquid-gas interfaces. An equilibrium of the tension forces is [16]:

$$\sigma_{sg} = \sigma_{sl} + \sigma_{lg}\cos\theta \tag{2}$$

The parameters determining the rivulet geometry are thickness δ_o and width W, which are both related to R and θ.

$$W = 2R\sin\theta \tag{3}$$

$$\delta_o = R(1-\cos\theta) \tag{4}$$

2.1 Calculation of Water Film Flow

2.1.1 Mass Conservation of Water Film

As shown in Fig. 3, two regions above the surface are taken into account: the boundary layer region of the external air flow and the runback water region. The water flow on the anti-icing surface is subject to mass, momentum and energy conservations. During modeling, it is assumed that there is no water-ice phase change within the film/rivulet flow on the anti-icing surface and both of the airflow and water film flow are incompressible and steady.

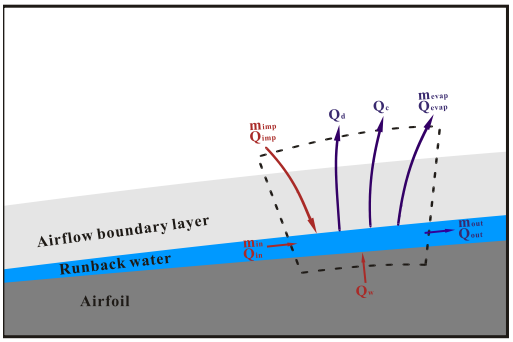

Fig. 3. Air Boundary and Water Flow on Anti-icing Surface

The mass conservation equation on the surface can be written as,

$$\dot{m}_{in}+\dot{m}_{imp}=\dot{m}_{out}+\dot{m}_{evap} \tag{5}$$

Where $\dot{m}_{imp}$ and $\dot{m}_{evap}$ represent the mass rate of impingement and evaporation, respectively. They can be computed by,

$$\dot{m}_{imp}=LWC\cdot\beta\cdot u_{\infty}\cdot ds \tag{6}$$

$$\dot{m}_{evap}=\frac{0.622h_c}{C_{p,air}}\left(\frac{P_{v,w}-P_{v,e}}{P_e-P_{v,w}}\right)\cdot ds \tag{7}$$

where β is the local collection efficiency. LWC is the liquid water content. $P_{v,w}$ and $P_{v,e}$ refer to the saturated vapor pressures at the water film temperature and the temperature of boundary layer edge, respectively. P_e is the edge pressure of boundary layer. h_c is the convective heat transfer coefficient of the external airflow on the airfoil surface.

The difference of the mass rate between the inlet and outlet of the control volume can be obtained by,

$$\dot{m}_{in}-\dot{m}_{out}=-\left[\frac{\partial}{\partial s}\left(\int_0^{\delta_1}\rho_{water}u_{water}dy\right)ds\right] \tag{8}$$

So Eq. (5) can be simplified as follows,

$$\begin{aligned}&\frac{0.622h_c}{C_{p,air}}\left(\frac{P_{v,w}-P_{v,e}}{P_e-P_{v,w}}\right)\cdot ds-LWC\cdot\beta\cdot u_{\infty}\cdot ds\\&=-\frac{\partial}{\partial s}\left(\int_0^{\delta_1}\rho_{water}u_{water}dy\right)\cdot ds\end{aligned} \tag{9}$$

where u_{water} is the velocity distribution in the boundary layer of the water film and δ_1 is the water film thickness.

2.1.2 Momentum Equation of Water Film

The movement of the water film on the airfoil surface is driven by the aerodynamic shear forces and the pressure gradient, as well as the viscous stress from the surface. Thus, the resultant force for the control volume of the film along the *s* axis is

$$\begin{aligned}F_{s-water}&=p\delta_1-\left(p+\frac{\partial p}{\partial s}ds\right)\left(\delta_1+d\delta_1\right)\\&+\left(p+\varepsilon\frac{\partial p}{\partial s}ds\right)d\delta_1-\tau_0 ds+\tau_{air}ds\end{aligned} \tag{10}$$

where p is the pressure above the airfoil surface; $\partial p/\partial s$ is the pressure gradient; ε is the increment coefficient of the pressure gradient. In addition, τ_0 is the viscous stress on the airfoil surface, and τ_{air} is the driven shear force from the air on the air-water interface. Since ε can be supposed to be an infinitesimal, the second order differential term in Eq. (10) can be neglected. This allows Eq. (10) to be rewritten as follows:

$$F_{s-water}=\left(-\delta_1\frac{\partial p}{\partial s}-\tau_0+\tau_{air}\right)ds \tag{11}$$

For the control volume of the water film, the net momentum flux at the inlet and outlet is

$$\dot{M}_{in}-\dot{M}_{out}=-\frac{\partial}{\partial s}\left(\int_0^{\delta_1}\rho_{water}u_{water}^2dy\right)ds \tag{12}$$

According to the moment conservation, the momentum equation can be written as:

$$\begin{aligned}&\left(-\delta_1\frac{\partial p}{\partial s}-\tau_0+\tau_{air}\right)\cdot ds=\dot{m}_{evap}u_{\delta_1}\\&-\dot{m}_{imp}u_{\infty,s}+\frac{\partial}{\partial s}\left(\int_0^{\delta_1}\rho_{water}u_{water}^2dy\right)\cdot ds\end{aligned} \tag{13}$$

where u_{δ_1} is the velocity of the water film at the air-water interface; $u_{\infty,s}$ is the velocity of the free stream along *s* direction.

The velocity distribution in the water film can be approximated as a polynomial function of y at a given location along the airfoil surface. The water film boundary conditions are

$$y=0:u_{water}=0 \tag{14}$$

$$y=\delta_1: u_{water}=u_{\delta_1};$$
$$\mu_{water}\left.\frac{du_{water}}{dy}\right|_{y=\delta_1}=\mu_{air}\left.\frac{du_{air}}{dy}\right|_{y=\delta_1}=\tau_{air} \quad (15)$$

Therefore, the velocity distribution in the water film boundary layer can be written as follows:

$$u_{water}=\left(\frac{2u_{\delta_1}}{\delta_1}-\frac{\tau_{air}}{\mu_{water}}\right)y+\left(\frac{\tau_{air}}{\delta_1\cdot\mu_{water}}-\frac{u_{\delta_1}}{\delta_1^2}\right)y^2 \quad (16)$$

2.1.3 Energy Balance of Water Film

An energy balance in the control volume includes the kinetic energy of the impinging water droplets Q_{imp}; the heat conduction from the airfoil surface Q_w; the evaporative energy of water Q_{evap}; the sensible heat by the incoming water droplets Q_d; the heat convection Q_c and the enthalpy through the water film in the flow direction Q_{in} and Q_{out}. According to the first law of thermodynamics, the energy balance equation produces:

$$Q_{imp}+Q_{in}+Q_w=Q_{out}+Q_{evap}+Q_c+Q_d \quad (17)$$

Each term can be expressed as following:

$$Q_{imp}=\dot{m}_{imp}\cdot\frac{u_{\infty,s}^2}{2} \quad (18)$$

$$Q_w=-\lambda_{water}\left.\frac{\partial T_{water}}{\partial y}\right|_{y=0}\cdot ds \quad (19)$$

$$Q_{evap}=\dot{m}_{evap}\cdot L_e \quad (20)$$

$$Q_c=h_c(T_{w-s}-T_\infty)\cdot ds \quad (21)$$

$$Q_d=\dot{m}_{imp}\cdot C_{p,water}\cdot\left(T_{w-s}-T_d\right) \quad (22)$$

$$Q_{out}-Q_{in}=\frac{\partial}{\partial s}\left(\int_0^{\delta_1}\rho_{water}u_{water}C_{p,water}\left(T_{water}-T_\infty\right)dy\right)\cdot ds \quad (23)$$

where $T_{w\text{-}s}$ is the temperature of the water film surface; T_{water} is the temperature in the boundary layer of water film. The thermal boundary conditions are:

$$y=0: T_{water}=T_{wall} \quad (24)$$

$$y=\delta_1: T_{water}=T_{w-s} \quad (25)$$

The temperature distribution can be obtained.

$$T_{water}=T_{wall}+\frac{T_{w-s}-T_{wall}}{\delta_1}y \quad (26)$$

Then, the energy balance equation can be rewritten as:

$$\frac{\partial}{\partial s}\left(\int_0^{\delta_1}\rho_{water}u_{water}C_{p,water}\left(T_{water}-T_\infty\right)dy\right)=-\lambda_{water}\frac{T_{w-s}-T_{wall}}{\delta_1}-h_c\left(T_{w-s}-T_a\right)+\left(LWC\cdot\beta\cdot u_\infty\right)\cdot\left[\frac{u_{\infty,s}^2}{2}-C_{p,water}\cdot\left(T_{w-s}-T_d\right)\right]-\frac{0.622h_c}{C_{p,air}}\left(\frac{P_{v,w}-P_{v,e}}{P_e-P_{v,w}}\right)\cdot Le \quad (27)$$

2.1.4 Momentum Equation of External Airflow Boundary Layer

The thickness of the control volume for the air boundary layer is δ_2. According to the mass conservation, the mass flux through the control volume in the external airflow boundary can be written as:

$$\dot{m}_{air}=\int_{\delta_1}^{\delta_1+\delta_2}\rho_{air}u_{air}dy-\left[\int_{\delta_1}^{\delta_1+\delta_2}\rho_{air}u_{air}dy+\frac{\partial}{\partial s}\left(\int_{\delta_1}^{\delta_1+\delta_2}\rho_{air}u_{air}dy\right)ds\right] \quad (28)$$

Then, the momentum flux through the control volume along s axis is

$$\dot{M}_{s-air}=\dot{m}_{air}u_e=-u_e\frac{\partial}{\partial s}\left(\int_{\delta_1}^{\delta_1+\delta_2}\rho_{air}u_{air}dy\right)ds \quad (29)$$

The resultant force for the control volume along s axis is

$$F_{s-air} = p\delta_2 - \left(p + \frac{\partial p}{\partial s} ds \right)\left(\delta_2 + d\delta_2\right) + \left(p + \varepsilon \frac{\partial p}{\partial s} ds \right) d\delta_2 - \tau'_{air} ds \quad (30)$$

where τ'_{air} is the reacting force of τ_{air}. Simplifying Eq. (30), it should be rewritten as:

$$F_{s-air} = \left(-\delta_2 \frac{\partial p}{\partial s} - \tau'_{air} \right) ds \quad (31)$$

Thus, the momentum equation can be expressed as:

$$-\left(\tau'_{air} + \delta_2 \frac{\partial p}{\partial s} \right) ds = \left[\int_{\delta_1}^{\delta_1+\delta_2} \rho_{air} u_{air}^2 dy + \frac{\partial}{\partial s}\left(\int_{\delta_1}^{\delta_1+\delta_2} \rho_{air} u_{air}^2 dy \right) ds \right] - \int_{\delta_1}^{\delta_1+\delta_2} \rho_{air} u_{air}^2 dy - u_e \frac{\partial}{\partial s}\left(\int_{\delta_1}^{\delta_1+\delta_2} \rho_{air} u_{air}^2 dy \right) ds \quad (32)$$

That is,

$$\tau'_{air} + \delta_2 \frac{\partial p}{\partial s} = u_e \frac{\partial}{\partial s}\left(\int_{\delta_1}^{\delta_1+\delta_2} \rho_{air} u_{air} dy \right) - \frac{\partial}{\partial s}\left(\int_{\delta_1}^{\delta_1+\delta_2} \rho_{air} u_{air}^2 dy \right) \quad (33)$$

As well, the velocity distribution is assumed as a polynomial, the boundary conditions for the airflow are:

$$y = \delta_1 : u_{air} = u_{\delta_1} \quad (34)$$

$$y = \delta_1 + \delta_2 : u_{air} = u_e, \frac{\partial u_{air}}{\partial y} = 0 \quad (35)$$

Then, the velocity distribution can be expressed as:

$$u_{air} = u_e - \frac{u_e - u_{\delta_1}}{\delta_2^2}\left(\delta_1 + \delta_2\right)^2 + 2\frac{u_e - u_{\delta_1}}{\delta_2^2}\left(\delta_1 + \delta_2\right) y - \frac{u_e - u_{\delta_1}}{\delta_2^2} y^2 \quad (36)$$

Then the shear force at the air-water interface is determined by:

$$\tau'_{air} = \mu_{air} \left. \frac{du_{air}}{dy} \right|_{y=\delta_1} \quad (37)$$

The mass, momentum, energy equations of the water film and the momentum equation of the external airflow boundary layer are solved simultaneously. A finite difference method is used in the solution. The thickness and velocity distribution of the water film along the airfoil surface can be obtained by iteration.

2.2 Calculation of Rivulet Flow

When a transition from water film flow to rivulet flow occurs, the mass conservation and energy conservation should be:

$$\dot{m}_f = \dot{m}_r \quad (38)$$

$$E_f = E_r \quad (39)$$

where the subscripts *f* and *r* represent the water film and rivulet, respectively.

The mass flow rates per width *L* for the film and rivulet flow are:

$$\frac{\dot{m}_f}{L} = \int_0^{\delta_f} \rho_{water} u_f(y) dy \quad (40)$$

$$\frac{\dot{m}_r}{L} = \frac{2}{L} \int_0^{R\sin\theta} \int_0^{\eta(z)} \rho_{water} u_r(z, y) dy dz \quad (41)$$

where $u_f(y)$ and $u_r(z,y)$ are the velocity distributions of the film and rivulet flow, respectively.

According to mass conservation, Eq. (40) equals to Eq. (41). Then

$$L = \frac{2R^3 \varphi(\theta)}{\delta_f^2} \quad (42)$$

where,

$$\varphi(\theta) = \sin\theta - \frac{1}{3}\sin^3\theta - \theta\cos\theta \quad (43)$$

The total mechanical energy is the sum of the surface energy and the kinetic energy. Therefore, the total mechanical energy for the film and rivulet can be respectively expressed as:

$$\frac{E_f}{L}=\int_0^{\delta_f}\frac{1}{2}\rho_{water}u_f^2(y)dy+\sigma_{sl}+\sigma_{\lg} \tag{44}$$

$$\begin{aligned}\frac{E_r}{L}&=\frac{2}{L}\int_0^{R\sin\theta}\int_0^{\eta(z)}\frac{1}{2}\rho_{water}u_r^2(z,y)dydz\\&+\frac{2R\sin\theta}{L}\sigma_{sl}+\frac{2R\theta}{L}\sigma_{\lg}+\frac{L-2R\sin\theta}{L}\sigma_{sg}\end{aligned} \tag{45}$$

According to the energy conservation,

$$\begin{aligned}&\frac{\rho_{water}\tau_{water}^2}{6\mu_{water}^2}\frac{\phi(\theta)}{\varphi(\theta)}\delta_f^2R^3\\&+(\sigma_{\lg}\cos\theta-\sigma_{\lg}-\frac{\rho_{water}\tau_{water}^2\delta_f^3}{6\mu_{water}^2})R^2\\&+\frac{2\theta-\sin2\theta}{2\varphi(\theta)}\delta_f^2\sigma_{\lg}=0\end{aligned} \tag{46}$$

where,

$$\begin{aligned}\phi(\theta)==&\frac{1}{32}(36\theta-28\sin2\theta\\&-\sin4\theta+24\theta\cos2\theta)\end{aligned} \tag{47}$$

Setting a dimensionless film thickness and radius as following, respectively:

$$\delta^+=\frac{\delta_f^3}{\left[\frac{6\mu_{water}^2\sigma_{\lg}}{\rho_{water}\tau_{water}^2}\right]} \tag{48}$$

$$R^+=\frac{R^3}{\left[\frac{6\mu_{water}^2\sigma_{\lg}}{\rho_{water}\tau_{water}^2}\right]} \tag{49}$$

Substituting Eq. (48) and (49) into Eq. (47), then the energy conservation can be rewritten as:

$$\begin{aligned}&\frac{\phi(\theta)}{\varphi(\theta)}\left[\delta^+\right]^{2/3}R^+ +(\cos\theta-1-\delta^+)\left[R^+\right]^{2/3}\\&+\frac{2\theta-\sin2\theta}{2\varphi(\theta)}\left[\delta^+\right]^{2/3}=0\end{aligned} \tag{50}$$

The film will break up at the impingement limit according to the minimum total energy (MTE) criterion [17]. However, the experiment results show that the breakup occurs behind the impingement limit [18]. So the experimental results of the film thickness at breakup position are used in calculating the rivulet shape.

3 Computational Results

The experimental cases from the reference has been chosen to validate the mathematical model. Zhang et al. [18] developed a digital image projection (DIP) method to achieve quantitative measurement of the thickness distributions of the surface water film/rivulet flow on a NACA 0012 airfoil. Under the same conditions, the numerical results agree well with the experimental data both in orders of magnitude and trends [19].

Then on this basis, the effect of contact angle is taken into consideration in this paper. The experimental airfoil model and conditions are still used in the numerical calculation. The chord length of the airfoil model is 101mm. The ambient temperature and airfoil surface temperature are both set as 20 ^{o}C. Medium volume diameter (MVD) of the droplets is 20 μm and liquid water content (LWC) is 10 g/m^3. Cases under different contact angles are studied when the free stream velocities are 20 m/s and 25 m/s. The contact angles are 80 °, 90 °, 100 °, 110 ° and 120 °, respectively.

3.1 Results of the Flow Field and Local Collection Efficiency

The flow field around the airfoil is obtained by ANSYS FLUENT. The computing mesh is about 63000 and the mesh dependent study has been conducted. The velocity and pressure distributions around the airfoil can be obtained when completing the flow field computation. After that, the water impingement characteristics are calculated by using Eulerian approach. The local collection efficiency results under each calculation condition are shown in Fig. 4. The computation of the flow field and local collection efficiency have little to do with the contact angle but mostly depend on the free stream velocity. Thus, the local collection efficiency maintains a consistent distribution under the conditions of same free stream velocity and different contact angles.

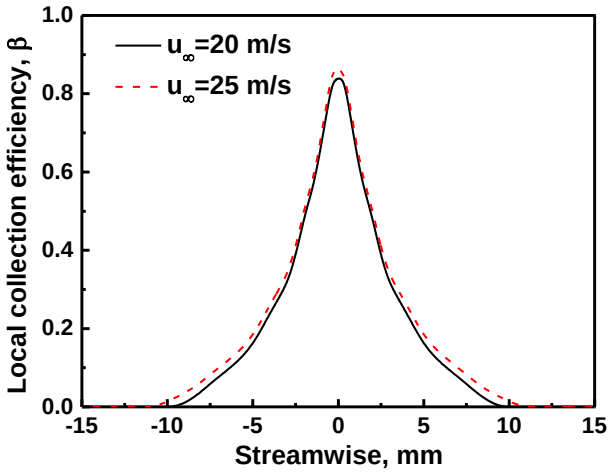

Fig. 4. Local Collection Efficiency Distribution

3.2 Results of Water Film Flow

The film thickness distributions under each calculation condition are shown in Fig. 5. From the governing equations of water film in the mathematical model, the contact angle has no influence on the film flow. However, the impingement region and the local collection efficiency are both increasing when the free stream velocity raises from 20 m/s to 25 m/s, as shown in Fig. 4. It indicates that more droplets impinge on the surface and the impingement mass flux per unit area will increase with the higher free stream velocity, as shown in Fig. 6.

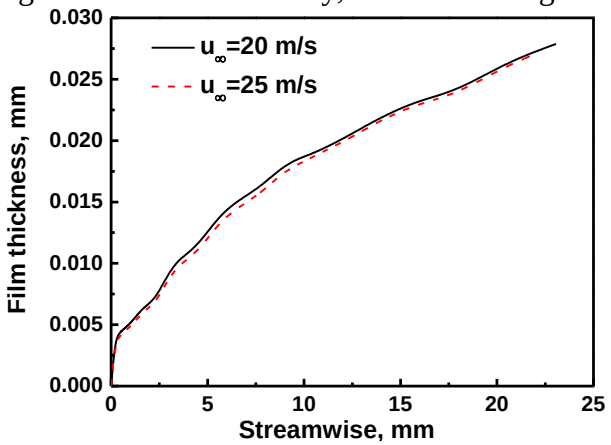

Fig. 5. Film Thickness Distributions

On the other hand, the film flow near the leading edge is more easily affected by the shear force generated by the air flow. Synthesizing these two reasons, the film thickness at velocity of 25 m/s is slightly smaller than that at velocity of 20 m/s and the difference will gradually disappear when water film flows out of the impingement region. In addition, the breakup position at the velocity of 25 m/s is closer to the stagnation point and the film thickness there is smaller than that at the velocity of 20 m/s, which can bring great impacts on the formation of rivulets.

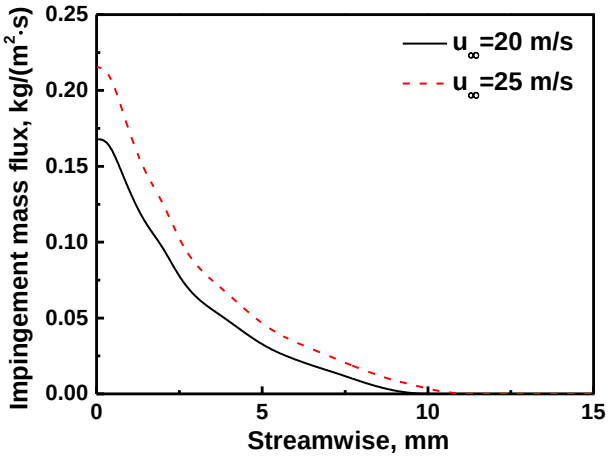

Fig. 6. Impingement Mass Flux Distribution

3.3 Results of Rivulet Flow

According to the equations of rivulet flow, the contact angle has a significant influence on the rivulet shape. Firstly, the dimensionless rivulet radium R^+ can be solved by using Eq. (50), as shown in Fig. 7. The R^+ has an obvious decrease when the contact angle increases at the same free stream velocity and tends to be constant when the contact angle reaches to 120 °. When the effect of free stream velocity is considered, the R^+ at the velocity of 25 m/s is larger than that at 20 m/s while the difference between the two velocities is gradually narrowing with the contact angle increasing.

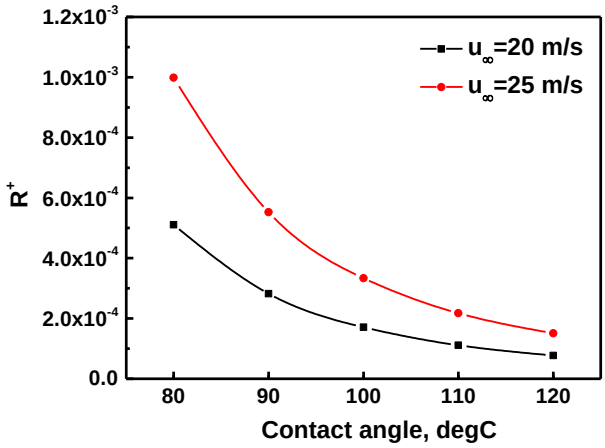

Fig. 7. Dimensionless Rivulet Radius Distribution

Then, based on Eq. (49), the rivulet radium R can be calculated through the value of R^+, as shown in Fig. 8. Since the physical properties and

surface shear force of the film/rivulet remain unchanged at the same free stream velocity, the R keeps a downward trend as the R^+ when the contact angle raises from 80 ° to 120 °. Since the increasing of the free stream velocity leads to the growth of the surface shear force, the R becomes smaller instead at larger free stream velocity. According to Eq. (3) and Eq. (4), the R and contact angle jointly determine the rivulet shape.

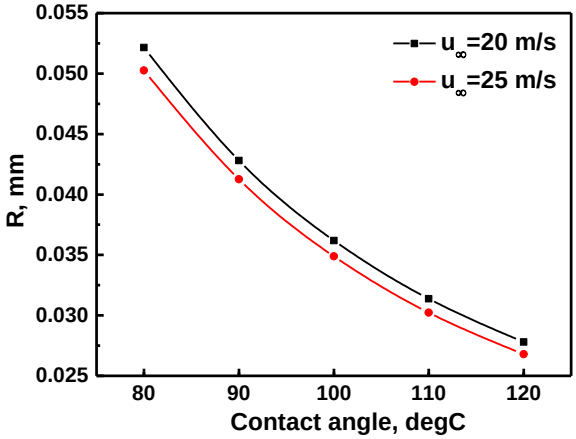

Fig. 8. Rivulet Radius Distribution

Fig. 9 and Fig. 10 are the rivulet width and thickness under different contact angle at free stream velocity of 20 m/s and 25 m/s, respectively. In general, both of the rivulet width and thickness decrease with the increase of contact angle while the width change is more sensitive to the contact angle than the thickness. As shown in Fig. 9, there is a significant decline in the rivulet width with the contact angle increasing at the same free stream velocity. When the contact angle equals to 80 °and 90 °, the values of sinθ in Eq. (3) are both close to 1 so that the rivulet width distributions under the two θs are almost depending on the value of R. When the contact angle reaches to 120 °, the value of sinθ, as well as the value of R, is the smallest so that the width narrows down obviously. In addition, the rivulet width at the free stream velocity of 20 m/s is larger than that at the velocity of 25 m/s under different contact angles. And the difference at the two different velocities tends to reduce with the contact angle increasing.

As shown in Fig. 10, the rivulet thickness falls in a small range when the contact angle raises at the same free stream velocity. The reason is that the value of (1-cosθ) in Eq. (4) is increasing while the value of R is decreasing with the contact angle increasing so that the influences on the rivulet thickness from the two are almost cancelled out. On the other hand, the variation trends with the contact angle at two different free steam velocities remain fairly consistent as the distributions of R.

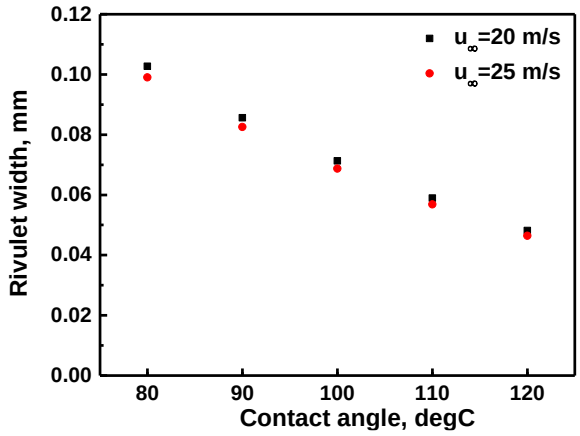

Fig. 10. Rivulet Width Distribution

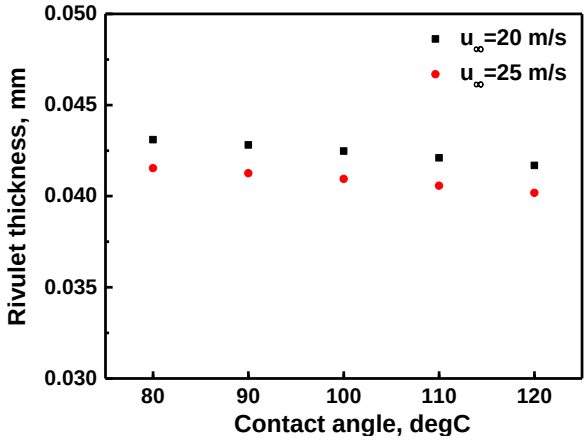

Fig. 11. Rivulet Thickness Distribution

4 Conclusions

A mathematical model is developed to analyze the characteristics of the runback water flow and heat transfer on anti-icing airfoil surface. The criterion of water flow evolution is presented to predict the shape of the rivulets on the airfoil anti-icing surface. The effects of the free stream velocity and contact angle are considered. The results show that the higher free stream velocity leads to a slightly thinner film flow near the leading edge on the anti-icing surface, generating the smaller thickness and width of rivulet after film breakup. The contact angle has an obvious influence on the rivulet width. That is, the larger contact angle is, the smaller rivulet width becomes. As well, the rivulet thickness has a small reduction with the increase of contact angle.

When the contact angle increases, the influence of free stream velocity on the rivulet shape are almost cancelled out. The rivulet widths under two velocities are nearly equal and the difference of rivulet thickness remains the same.

References

[1] Kind R J, Potapczuk M G, Feo A, Golia C and Shah A D. Experimental and computational simulation of in-flight icing phenomena. *Progress in Aerospace Science*, Vol. 34, pp 257-345, 1998.

[2] Naterer G F. Coupled liquid film and solidified layer growth with impinging supercooled droplets and joule heating. *International Journal of Heat and Fluid Flow*, Vol. 24, No. 2, pp 223-235, 2003.

[3] Nelson J J, Alving A E and Joseph D D. Boundary layer flow of air over water on a flat plate. *Journal of Fluid Mechanics*, Vol. 284, No. 1, pp 159-169, 1995.

[4] Tsao J C, Rothmayer A P and Anatoly I R. Stability of air flow past thin liquid films on airfoils. *Computers & fluids*, Vol. 26, No. 5, pp 427-452, 1997.

[5] Rothmayer A P. Scaling laws for water and ice layers on airfoils. *41st Aerospace Sciences Meeting & Exhibit*, Reno, AIAA Paper 2003-1217, 2003.

[6] Ueno K and Farzaneh M. Linear stability analysis of ice growth under supercooled water film driven by a laminar airflow. Physics of Fluids, Vol. 23, pp 042103, 2011.

[7] Silva G A L, Silvares O and Jesus E J G. Numerical simulation of airfoil thermal anti-ice operation part 1: mathematical modeling. *Journal of Aircraft*, Vol. 44, No. 2, pp 627-634, 2007.

[8] Nicholas P D. Numerical analysis of de-icing fluid flow off from aircraft wings. *AIAA Atmospheric and Space Environments Conference*, Toronto, AIAA Paper 2010-7838, 2010.

[9] Rothmayer A and Tsao J. Water film runback on an airfoil. *38th Aerospace Sciences Meeting & Exhibit*, Reno, AIAA Paper 2000-0237, 2000.

[10] Al-Khalil K M, Keith Jr T G and Witt K J. Development of an improved model for runback water on aircraft surfaces. *Journal of Aircraft*, Vol. 31, No. 2, pp 271-278, 1994.

[11] El-Genk M S and Saber H H. Minimum thickness of a flowing down liquid film on a vertical surface. *International Journal of Heat and Mass Transfer*, Vol. 44, pp 2809-2825, 2001.

[12] El-Genk M S and Saber H H. An investigation of the breakup of an evaporating liquid film, falling down a vertical, uniformly heated wall. *Journal of Heat Transfer*, Vol. 124, No. 1, pp 39-50, 2002.

[13] Saber H H and El-Genk M S. On the breakup of a thin liquid film subject to interfacial shear. *Journal of Fluid Mechanics*, Vol. 500, pp 113-133, 2004.

[14] Silva G A L, Silvares O and Jesus E J G. Water film breakdown and rivulets formation effects on thermal anti-ice operation simulation. *9th AIAA/ASME Joint Thermophysics and Heat Transfer Conference*, San Francisco, AIAA Paper 2006-3785, 2006.

[15] Silva G A L, Silvares O, Jesus E J G, et al. Differential boundary-layer analysis and runback water flow model applied to flow around airfoils with thermal anti-ice. *1st AIAA Atmospheric and Space Environments Conference*, San Antonio, AIAA Paper 2009-3967, 2009.

[16] Davies J T and Rideal E K. Interfacial phenomena, 2nd Edition. *Academic Press*, NY, 1963.

[17] Al-Khalil K M. Numerical simulation of an aircraft anti-icing system incorporation a rivulet model for the runback water. Ph. D. Thesis, Univ. of Toledo, OH, 1991.

[18] Zhang K, Blake J, Rothmayer A and Hu H. An experimental investigation on wind-driven rivulet/film flows over a NACA0012 airfoil by using digital image projection technique. *52nd Aerospace Sciences Meeting*, Maryland, AIAA Paper 2014-0741, 2014.

[19] Dong W, Zheng M, Zhu J, and Lei G. Calculation and analysis of runback water flow on anti-icing airfoil surface. *Journal of Aircraft*, Vol. 53, No. 6, pp 1597-1605, 2016.

5 Acknowledgement

The authors at Shanghai Jiao Tong University were supported by 973 program under Grant No. 2015CB755800 and the National Natural Science Foundation of China under Grant No. 11572195.

6 Contact Author Email Address

Mailto: wdong@sjtu.edu.cn

Copyright Statement